Design and structural modelling of patient-specific 3D-printed knee femur and tibia implants

Bolugoddu Sandeep[1], Saravanan Dhanushkodi[2], Sudhakar Kumarasamy[3]
[1]Department of Mechanical Engineering, Prist Deemed University, Thanjavur, India
[2]Department of Mechanical Engineering, Ponnaiyah Ramajayam Institute of Science and Technology, Vallam, India
[3]Department of Mechanical Engineering, University Malaysia Pahang, Pahang, Malaysia

Article Info	ABSTRACT
	Arthritis is a degenerative joint condition that progressively damages the knee, leading to pain, stiffness, and limited mobility. To alleviate these symptoms and restore joint functionality, total knee arthroplasty (TKA) is performed. This procedure becomes necessary due to either sudden trauma to the knee or gradual wear and tear of the meniscus and cartilage. TKA involves meticulous planning, precise bone cutting, and the placement of prosthetic components made from high-density polyethylene and metal alloys. However, traditional methods creating customized knee implants are expensive and time-intensive. This study explores the challenges in manufacturing personalized knee implants for TKA and evaluates the potential of three-dimensional (3D) printing technology in this process. Variations in knee joint anatomy across populations complicate surgery, as optimal outcomes rely on precise alignment and implant dimensions. A preoperative computed tomography (CT) scan identifies the region of interest (ROI), such as the knee joint. The scan data is then processed using computer-aided design (CAD) software to generate a printable file. The patient's CT scan data is converted into a standard triangulation language (STL) file and CAD models of the knee joint. Errors such as overlapping triangles or open loops in the STL file are corrected, and unwanted geometries near the ROI are removed. Resection techniques are applied to create CAD models tailored to the patient's bone morphology. Fused deposition modeling (FDM) is then used to produce prototypes of the knee joint and implants. Despite visible layer lines in the printed prototypes, challenges encountered during the process were effectively resolved. *This is an open access article under the CC BY-SA license.*

Corresponding Author:

Bolugoddu Sandeep
Department of Mechanical Engineering, Prist Deemed University
Thanjavur, Tamil Nadu, India
Email: sandeepvarma@jits.in

1. INTRODUCTION

Knee arthritis, including osteoarthritis, rheumatoid arthritis, and post-traumatic arthritis, is a common condition affecting the knee joint [1]. Over the last four decades, knee replacement surgeries have increased globally [2]. Total knee replacement (TKR) is often required due to cartilage and bone degeneration, joint swelling, and mild synovial inflammation caused by osteoarthritis [3]. Despite its success, up to 25% of TKR patients report dissatisfaction [4].

As shown in Figure 1, understanding knee anatomy and injury mechanisms is crucial for effective diagnosis and treatment [5]. The knee joint consists of the femur (thigh bone), tibia (shin bone), and the kneecap (patella). These bones are covered by a smooth layer called articular cartilage, which enables smooth

movement within the joint. Between the femur and tibia, there are C-shaped structures called menisci that act as shock absorbers for the knee. Typically, the knee is understood to include the tibiofemoral and patellofemoral joints. The tibiofemoral joint is divided into medial and lateral sections. While there is a slight difference in the size of the lateral and medial condyles, the former is generally constant. During flexion, the femoral and tibial condyles can slide and roll together.
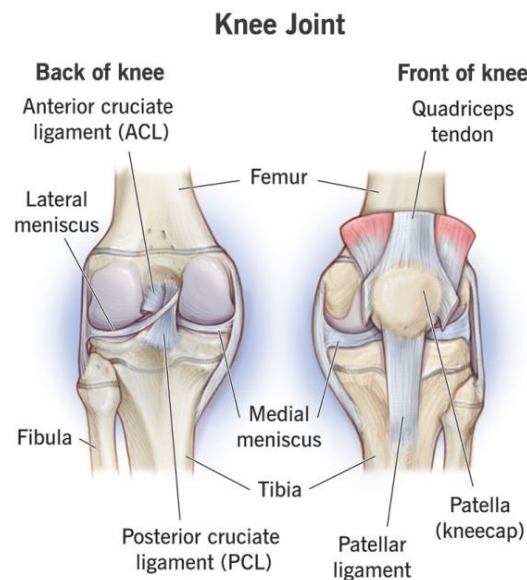

Figure 1. Anatomy of the knee

Direct knee impacts require immediate attention [6], and prostheses have a reported 10-year survival rate exceeding 95%. Precision in bone cuts and prosthetic placement is key to successful TKR outcomes. total knee arthroplasty (TKA) evenly distributes knee joint load to reduce polyethylene liner wear and enhance prosthesis durability [7]. Advances in three-dimensional (3D) printing have made it a valuable tool in orthopedics, aiding in mobility restoration and pain reduction for improved patient quality of life [8]. Despite its benefits, increased arthroplasty procedures lead to many complications, but improving TKA with 75% to 89% patient satisfaction, around 50% report functional limitations or infections. Additional wear from tibial bearing micro-motion and ultra-high-molecular-weight polyethylene (UHMWPE) impacts further contribute to challenges [9].

Patient-specific instrumentation (PSI) in TKA simplifies surgery, enhances cutting accuracy, and reduces complications. It also decreases instrument use, shortens procedures, and lowers costs [10], [11]. Using CT or MRI scans, 3D printing creates anatomically customized cutting guides based on detailed models of the patient's knee, enabling precise pre-operative planning. Surgeons use these guides, made from materials like nylon, polymers, or metals, to determine key surgical parameters such as alignment, rotation, resection levels, and component sizing [12]–[14]. During surgery, PSI guides assist in bone cuts and pin positioning. If adjustments are needed, standard instruments are used. Producing these guides typically takes about three weeks [15]. Proper soft tissue handling and osteophyte retention are crucial for guide placement. MRI-based systems do not require cartilage removal, while CT-based systems do.

This research aims to develop an innovative knee joint consisting of femur bone, tibia bone, and kneecap (patella) using 3D-printed polylactic acid (PLA), offering a lightweight, user-friendly design for patient rehabilitation. The study examines the performance of the PLA key components under stress and strain, comparing the effectiveness of these two commercially available materials. Advancements in 3D-printed polymer components have made them suitable for demanding applications, with reduced printing costs making them a viable alternative to traditional orthotics. Early prototypes were bulky due to limitations in older technology, but now 3D-printed braces offer personalized, comfortable, and functional solutions. Custom designs ensure a precise fit and improved patient compliance. The versatility of 3D printing allows for complex geometries and material selection to achieve the desired properties, while rapid prototyping enables quick modifications [16]–[23].

Medical applications require specialized materials, such as energy-absorbing, impact-resistant, and biologically modeling components. Recent research focuses on medicinal polymers with flexibility [24], [25], toughness [26], [27], electrical conductivity [28], [29], and biocompatibility [30], [31]. Fatigue fractures are often due to inadequate bone support, commonly from osteolysis. Precise component positioning during surgery is essential [32]. Fractures typically occur at the base plate and stem junction, requiring careful monitoring for subsidence, as this rare failure is difficult to detect on radiographs [33].

Kurenov *et al.* [34], the surgical impact of 3D-printed personalized bone plates for severe tibial plateau fractures. Jeon *et al.* [35] found that 3D printing-assisted TKA resulted in better short-term outcomes, improved surgical efficiency, and enhanced knee function compared to conventional TKA. Randazzo *et al.* [36] the human knee and analyzed biomechanical properties under different loading conditions. Saijo *et al.* [37] Pro/E software for 3D knee prosthesis reconstruction and evaluated stress distribution with finite element analysis (ANSYS). Huang and Zhang [38] discovered that scanning speed significantly affected the tensile strength of titanium alloy implants. Crafts *et al.* [39] found that the Taguchi method reduced buckling deformation in titanium alloy bracing structures. Chae *et al.* [40] customized 3D-printed stainless steel tibial implants for fracture fixation with surgical screws.

Williams *et al.* [41] studied toughness, combining strength and ductility, using tough polyurethane to create a 3D-printed tensile bar with crosshatch structures, comparing physical and chemical cross-linking methods. Advances in flexible materials now allow prosthetics to be customized to individual physiology using scanning and fitting technologies [42]. In one study, 3D mapping software created a nasal contour, printed with a Stratasys PolyJet printer and rubber-like Tango Plus material. Stereolithography has also been used to print complex patterns on flexible materials [43]. Biocompatibility is essential for materials in printed objects that interact with the body, ensuring they don't cause harm. Stratasys MED610, an acrylic-based polymer, is used to create tissue scaffolds with complex topologies. It meets key biocompatibility criteria, including biodegradability, non-cytotoxicity, and tissue stimulation [44].

From the above literature survey discussions, current knee implant modeling and molding methods, especially for tibial prostheses, have several limitations. This paper focuses on the modeling approach and FDM technique for personalized patient-specific 3D-printed knee femur and tibia implants. The knee joint consists of the femur, tibia, and patella, with articular cartilage enabling smooth movement. C-shaped menisci between the femur and tibia serve as shock absorbers. The knee has two main components: the tibiofemoral and patellofemoral joints. The tibiofemoral joint is divided into medial and lateral sections, with a slight size difference between the condyles.

As shown in Figure 2, in TKR surgery, diseased bone and cartilage are removed, and the femur and tibia are reshaped to fit the prosthesis components. The prosthesis includes femoral, tibial, and patellar parts. In TKR surgery, diseased bone and cartilage are removed. The distal femur and proximal tibia are cut and reshaped to accommodate the femoral component and tibial tray of the prosthesis. The three main components are the femoral, tibial, and patellar components. As shown in Figure 2, the tibial and patellar components can be made of solid polyethylene or have a metal backing that supports a polyethylene articulating surface.

TKA is often performed when the cartilage is damaged, the joint is misaligned, and worn cartilage surfaces need replacement with artificial components [45]. The primary goal of TKA is to resolve mechanical problems in the joint, rather than treat the underlying disease. For individuals with severe joint damage, arthroplasty may be the only available treatment [46].

Managing excess weight can further enhance post-surgery outcomes [47]. In 31% of cases, TKA resulted in weight loss, improved BMI, and better functionality [48]. Among 781 revision TKA patients, common failure causes included loosening (39.9%), infection (27.4%), instability (7.5%), periprosthetic fracture (4.7%), and arthrofibrosis (4.5%).
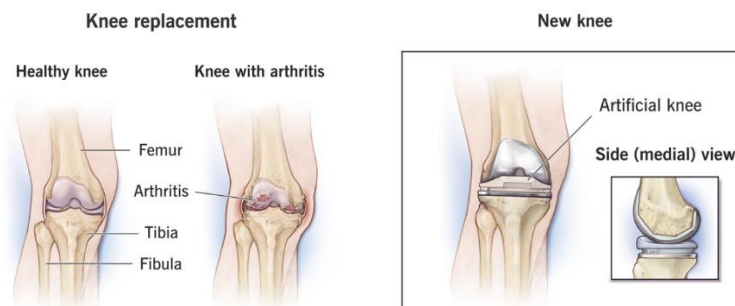

Figure 2. Components of TKA

2.   PROPOSED WORK: MATERIALS AND METHODS

The materials used are 3D printing material through a material extrusion process in additive manufacturing (AM) that creates objects by depositing material through a nozzle, layer by layer, based on computer-aided design (CAD) data [49], [50]. It is especially useful in biomedical devices and tissue engineering (TE) for producing custom, patient-specific parts [51], [52]. Fused deposition modeling (FDM) is a type of additive technology where material is melted and extruded to form shapes, building layers one at a time [53].

From the above literature survey, we have observed that the 3D modeling of human bones has become a transformative tool in medical research and education, with materials like PLA and recycled polyethylene terephthalate (rPET) emerging as popular choices due to their unique properties. Below is a detailed exploration of how these materials are fabricated and practically modeled for bone replicas. The properties of bone modeling of PLA are: derived from renewable resources like corn starch or sugarcane; biodegradable, environmentally friendly, and easy to print; and offers good rigidity, high dimensional accuracy, and smooth surface finishes, making it suitable for replicating bone structures. And for rPET are: made from recycled plastic, such as used beverage bottles; strong, durable, and less brittle compared to PLA; and provides a sustainable alternative with high strength and toughness, with the similar mechanical properties to bone.

The PLA fabrication process involves PLA granules that are produced through polymerization of lactic acid derived from biomass. The granules are melted and extruded into filament form, ready for use in 3D printers, and filaments come in various diameters (e.g., 1.75 mm or 2.85 mm) and colors for customized applications. The rPET fabrication process is: PET waste is collected, cleaned, and shredded into flakes; these flakes undergo extrusion to produce recycled PET filaments; and filaments are processed to maintain consistent quality, ensuring printability and strength.

The process in modeling human bones using PLA and rPET, has a pre-processing stage where z high-resolution CT scan or MRI of the human bone is obtained, the imaging data is processed using CAD software to create a 3D model, and the model is converted into a standard tessellation language (STL) file, which is used for 3D printing. In 3D printing stage the printing setup is performed through PLA or rPET filament is loaded into an FDM 3D printer and printer parameter (temperature, speed, and layer height) are adjusted based on the material. In the next stage printing process is performed through: for PLA, print temperatures range between 190-220 °C, rPET requires slightly higher temperatures (230-260 °C), and the model is printed layer by layer to replicate the bone structure, with support structures added as needed.

In the post-processing and finishing stage, supports are removed, and the model is sanded to achieve a smooth finish. PLA models may undergo annealing for increased strength and heat resistance, and rPET models can be treated with coatings for enhanced durability and surface texture. By leveraging the unique properties of PLA and rPET, 3D modeling of human bones can be tailored for diverse applications, from education to medical research, combining precision, practicality, and environmental consciousness.

Various software tools are used for diagnosing diseases and injuries. 3D Slicer, an open-source program, employs volume rendering to display 3D images. Figure 3 illustrates the degradation and recovery of joint space due to cartilage and meniscus damage [54], [55]. The tibial implant optimization (topological optimization) was done using finite element analysis and MATLAB software. The tailored implant model was imported into ANSIS and MATLAB simulation mechanical for stress analysis and parameter adjustment. The 3D tibial model was imported into MATLAB simulation professional and transferred to MATLAB simulation mechanical for finite element analysis. The model was partitioned into grids, with PLA material and constraint conditions applied. The proximal tibia was fixed, and a 20 N load was applied to the tibial articular surface. The analysis results revealed displacement at the articular surface border and stress concentration in the tibial tendon. Increasing tendon thickness and distribution could improve tibial strength and reduce stress concentration.

The parameter control table in MATLAB simulation of mechanical was used to adjust the tibial tendon's height and thickness, increasing its thickness and distribution area. The updated model was then confirmed. After grid partitioning, the model's material PLA, constraint conditions, loading, time step, and solution method were set for analysis. The optimized tibial implant's stress analysis demonstrated a reduction in maximal displacement from 0.00344 mm to 0.00043 mm and a decrease in maximal stress from 7.235 N/mm² to 1.165 N/mm². The optimized model exhibited reduced displacement strain, more uniform stress distribution, and improved tibial strength with reduced stress concentration. The designed tibial implant was imported into STL format, and positioned at a 90° inclination for standard placement. The part was sectioned into 1434 layers, each 0.034 mm thick, with a molding time of 5 hours.

To perform knee-joint-resection for patient-specific-implants, a resurfaced model for patient-specific knee components is created by bone excision in CAD, which is also utilized to evaluate off-the-shelf components [56]. Based on femur geometry, there are three conventional sizes for femoral resection; the size

of the resection is determined by the anterior-posterior (A-P) length [57]. With an average length of 51.061 mm, the A-P comes into the tiny group. The knee aligns mechanically when the valgus angle is 6°. An intramedullary reference system that is oriented with the medullary canal and at a 6° angle between the mechanical and anatomic axes is used to cut the femur. 10 mm is the depth of the distal femur cut [58], [59]. With typical distal medial and lateral thicknesses of 5.5 mm and posterior medial and lateral thicknesses of 5.3 mm and 5.8 mm, respectively, the knee-joint implant has a modest bone resection. The tibia is sliced at a 0° angle with the mechanical and anatomical axes parallel. The joint line remains unaltered when 13 mm of tibial bone is removed, enabling the use of a 13 mm polyethylene liner rather than a 9 mm one [60], [61].

Femoral A-P length classifications help in personalizing knee implants. Typically, these sizes are divided into groups based on the A-P length measurements. Each group reflects specific dimensions that match the natural variations in femur sizes among individuals. This classification ensures a better fit of the prosthesis, optimizing the performance and comfort for the patient. Accurate grouping is crucial for successful knee replacement surgeries, as it allows for precise alignment and articulation within the joint. The process of measuring and categorizing femoral A-P lengths thus plays a vital role in orthopedic surgical outcomes. The resection of the knee joint is categorized into three standard sizes according to the geometry of the femur at the resection site. The classification of femoral A-P lengths is presented in Table 1.

Table 1. Classification of knee-based classifications on sizes

Sizes	Length (mm)
Small	53 to 56
Medium	61 to 63
Large	74 to 76

Knee joint implants and the femoral bone resection profile are utilized to model patient-specific implants using MATLAB Simulation. The average implant thickness values are used to generate the femoral implant models. With a 9 mm tibial bone excision, the tibial implant is used like the tibia profile. The liner is inserted into the tibial tray after a resection profile is made on the upper surface. The liner has a 2 mm shell, and the tibial tray is extruded by 4 mm and 9 mm, respectively.

To simulate and model knee-joint-components in 3D-printing, MATLAB simulation is used to import knee implant files, configure process parameters, and add support structures to the tibia tray and femoral implant. Following validation, G-codes are produced by the program and exported to the 3D printer for printing. The proposed research examines the effects of 3D-printed PLA composite material on TKR. Combining PLA with recycled PET (rPET) has resulted in a stable, 3D-printable material that allows for the creation of porous and finely structured scaffolds. These scaffolds demonstrate osteogenic and anti-inflammatory properties. This 3D-printed material meets many of the requirements outlined in the literature. The student version of pro-engineer, also known as Creo, is used to set print parameters and slice the STL file after importing the 3D model. The orientation of the knee joint is adjusted within the print area. The printing variables are detailed in Table 2.

Table 2. Material parameters for 3D model design analysis

Material type	Layer height (mm)	Number of shells	Infill (%)	Infill type	Build time for femur and liner implant	Build time for tibia tray	Support structure
PLA	0.22	2	29	Hexagoal	2 h	60 min	Added

For this analysis report, the following specifications are used, after reviewing several research papers and publications. Polymer materials are typically created using biologically extruded 3D printing techniques. Both natural polymers and partially synthetic polymers can be easily converted into hydrogel biological inks, which mimic the hydrophilic properties and biocompatibility of biological tissues. Their mechanical properties can be adjusted to form stable 3D structures. Most biological inks reported are used in gas-phase environments in vitro, although liquid-phase suspended 3D printing is also being explored, limited to specific liquid-phase solvents. The actual application environment of biomaterials is complex, with various printed biomaterial components and cells offering different properties and functions. This study focuses on selecting polymer materials, biological printing cells, and their use in bone and cartilage repair. This review details each component's characteristics, providing a basis and progress of 3D printing applications in biological bone and cartilage, as shown in Tables 3 and 4.

Table 3. Material properties of cartilage

Properties	Value
Young's modulus	0.06-0.020 MPa
Poission's ratio	0.45-0.49
Shear modulus	0.020 MPa
Temperature	25 ºC
Density	1100 kg/m^3
Permeability	10^{-15} to 10^{-16} m^4/N
Material type	viscoelastic (porous)

Table 4. Material properties of bone

Properties	Value
Young's modulus	12600-19400 MPa
Poission's ratio	0.3-0.39
Shear modulus	4850-5700 Mpa
Operating temperature	25 ºC
Density	1800 kg/m^3
Material type	Solid
Tensile strength	50-135 MPa
Compressive strength	(-50) to (-250) MPa
Shear strength	65 MPa

The tensile properties of human bone and 3D-printed kneebone joints are crucial for assessing how effectively synthetic materials can replicate natural structures in orthopedic applications. Cortical bone, a type of human bone, demonstrates exceptional tensile strength and toughness due to its unique composite structure, which combines collagen fibers with hydroxyapatite mineral crystals. This natural composition allows bones to endure substantial stress while retaining flexibility and durability.

Recent advancements in 3D printing technology have enabled the fabrication of kneebone joints using materials such as PLA composites. These materials are selected for their biocompatibility, mechanical properties, and ease of processing. However, replicating the intricate microstructure and mechanical behavior of human bone remains a significant challenge.

3. RESULTS AND DISCUSSION

The orthosis design was carefully considered for mechanical integrity, using two polymer matrices: PLA and rPET, with two commercial brands for each. These materials were chosen for their affordability, availability, and suitability based on their properties. The DICOM data is imported into 3D Slicer with threshold values set at 152 (lower) and 2,923.60 (upper) for better bone visualization. Slicing and smoothing tools are used to eliminate unwanted geometries. While smoothing deals with tiny, invisible geometries, slicers eliminate larger apparent geometry. MATLAB Simulation is used to correct open loops in the knee joint that were present during the conversion from DICOM to STL.

After importing the knee joint STL file into MATLAB Simulation, orientations are changed to guarantee a smooth surface finish, reduce support, and increase accuracy. The print parameters include two shells, 20% hexagonal infill, and a 0.20 mm layer height. The print took four hours and twenty-six minutes with supports using biodegradable PLA. The femoral, tibial, and liner implants of the 3D-printed knee joint prototype are similarly made of PLA using a 3D FDM printer with 0.20 mm layer height, 25% infill, and two shells. The femur and liner took 2 hours to print, while the tibial tray took 60 minutes.

3.1. 3-D printed kneebone joint

As shown in Table 5, a comparison of the tensile properties of the materials used in this study with those of natural human bone and 3D-printed kneebone joints reveals only minor differences in energy dissipation. To enhance the performance of 3D-printed kneebone joints, composite materials like PLA blended with recycled rPET have been utilized, combined with advanced printing techniques. Incorporating bioactive ceramics or nanomaterials into the printing process can further improve mechanical properties and better mimic the hierarchical structure of natural bone.

Moreover, optimizing printing parameters—such as layer thickness and orientation—can significantly influence the tensile properties of the final printed part. These ongoing developments promise to create more effective and durable orthopedic implants, ultimately improving patient outcomes and advancing the field of biomedical engineering. The tensile pieces after 3D modeling were analyzed and processed for polishing by making the surface roughness at 4.3 micrometers, to analyze the tensile test process.

Table 5. Comparisons of human bone and 3-D printed kneebone joint

Human bone properties			3D printed properties		
Tensile	Compressive	Shear	Tensile	Compressive	Shear
150 Mpa	250 Mpa	450 Mpa	140 Mpa	250 Mpa	300 Mpa

The steps involved in modeling 3D-printed knee femur and tibia implants using PLA and rPET in the proposed work are:

a. Data acquisition
− MRI scans: patient-specific imaging data in DICOM format is collected. MRI scans are often preferred for higher resolution in capturing bone structures.
− Segmentation: the regions of interest (e.g., femur and tibia) are segmented using software, using ANSIS and MATLAB to isolate the bone structures.

b. 3D model creation
− Thresholding and masking: thresholding values are adjusted to focus on the bone areas, and masks are created to define the boundaries of the 3D models.
− Region growing and surface generation: tools ANSIS and 3D View are used to generate 3D surfaces of the bones from segmented data.
− Noise removal: tools 3D view and MATLAB are used to smooth and rectify geometrical errors such as open loops and unwanted artifacts.

c. Customization and implant design
− Reverse engineering: the natural curvature of the bones is captured, and adjustments are made to ensure the implant fits accurately. Tool ANSIS is used for detailed design alterations.
− Material assignment: the density of cortical and cancellous bone is analyzed to determine mechanical properties. Joints knee data from MRI scans is used to simulate material characteristics.

d. Preparation for 3D printing
− Conversion to STL: the finalized 3D models are converted to STL format for slicing and 3D printing.
− Slicing and process parameters: tool 3D slicer is used to set parameters: i) layer height: 0.20 mm for PLA, ii) infill pattern: hexagonal infill is used for lightweight strength, around 20–25%, and iii) support structures: added to ensure stability during printing.

e. 3D Printing
− Material selection: PLA, a biodegradable polymer, and rPET, a recycled material, are used for environmentally friendly and biocompatible printing.
− Printing process: the models are printed using FDM printers. Parameters such as printing speed and temperature are optimized for material type.
− Post-processing: support structures are removed, and the printed surfaces are cleaned and polished to ensure a smooth finish.

f. Verification and testing
− Dimensional accuracy: the printed implants are compared against the original CAD designs to ensure accuracy.
− Mechanical testing: implants are tested for strength and flexibility to ensure they meet biomechanical requirements.
− Prototyping and assembly: the femur, tibial tray, and liner are tested in assembly to confirm compatibility and functionality.

g. Clinical considerations
− Customization: patient-specific factors, such as bone morphology, are accounted for during design.
− Surgical adaptability: implants are designed to ease surgical procedures like TKA.

This approach enables the creation of customized, cost-effective, and environmentally sustainable knee implants. The femur and tibia are each divided into four distinct regions: F1 to F4 for the femur and T1 to T4 for the tibia, with F1 and T1 representing the most proximal regions and F4 and T4 the most distal. Data from the scans included measurements from the entire distal femur, the entire proximal tibia, and the subchondral regions of both the femur and tibia.

To perform the modeling of the proposed knee joint process, as shown in Figures 3(a)-(c), the CT or NMR scans of a 42-year-old woman with left knee osteoarthritis capture images of the disease site, which are then imported. The correct orientation is selected during the import process. As shown in Figure 3(d), for the 3D model, threshold segmentation is applied, and disconnected regions are further divided into subgroups to create a new mask. The soft tissue site is marked as the starting point, and the endpoint is identified once the line penetrates the bone, generating an intensity interface where the prominent area represents the threshold.

The segmented DICOM file is made into individual standard triangulation language (STL) files as shown in Figures 3(a)-(d).

After threshold segmentation, the images were processed with a morphological operation to remove small burrs and eliminate floating pixels through region growing. The method calculate 3D models is for 3D reconstruction, and the implant model was smoothed and denoised for optimization the tibial implant model was then imported into the STL editor for grid repair, denoising, smoothing, and bone cutting simulation, with the cutting line. The tibial implant bone-cutting model was imported into MATLAB software for forward design. The implant model was selected based on the bone cutting surface, and its components (stem, wing, plate, groove, and articular surface) were adjusted to fit the tibial surface.

(a)

(b)

(c)   (d)
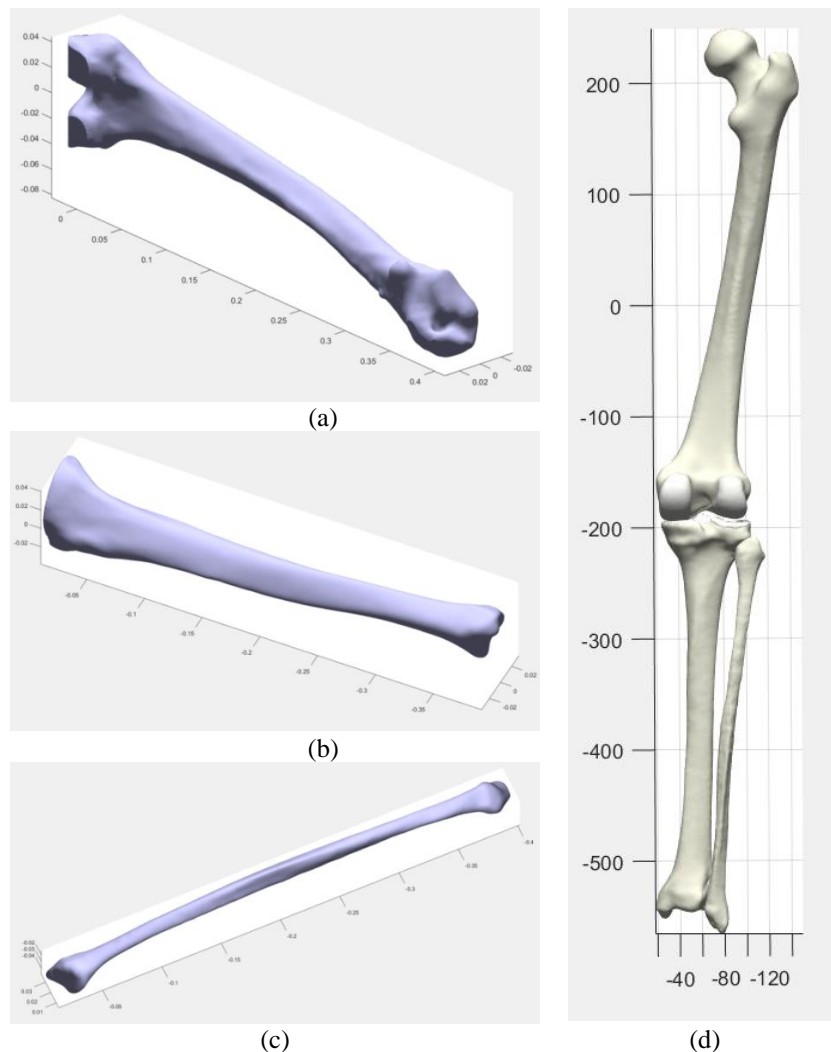
Figure 3. 3D model visualization of individual STL files of knee for proposed model implementation
(a) femur, (b) tibia, (c) fibula, and (d) femur, tibia, and fibula

Knee joint resection is standardized into three sizes based on femoral geometry at the resection site. The A-P length of the femur, shown in Figures 4(a) and (b), measures 53.351 mm medially and 56.796 mm laterally, averaging 55.072 mm, which classifies it as small. When the tibiofemoral angle, or "knee angle," is at 6° valgus, the knee aligns neutrally. Femur cutting follows the intramedullary reference system, guided by the medullary canal, aligning with the anatomical axis. This guide is angled at approximately 6° between anatomical and mechanical axes. The distal femur cut depth is 9 mm.

For its small size, the average bone resection thickness is 6.5 mm for distal medial and lateral sections, and 5.9 mm and 5.8 mm for posterior medial and lateral sections, respectively. These details are illustrated in Figure 4(c). With parallel mechanical and anatomical axes, the tibia is cut at a 0° angle.

Removing 11 mm of tibial bone maintains the joint line, allowing for an 11 mm polyethylene liner placement instead of 9 mm, as seen in Figure 4(d).

Table 6 shows the percentage values of strainT for all T and F across different attachment site combinations. The F2-T1 combination generally resulted in the lowest strainT, with two cases tying with F1-T1. However, in three cases, a different combination produced the lowest strainT, with no clear pattern identified. As no single combination consistently minimized strainT, the first hypothesis was further analyzed. The range, mean, and standard deviation of strainT for each combination were calculated to identify the most effective site, as detailed in Table 6.
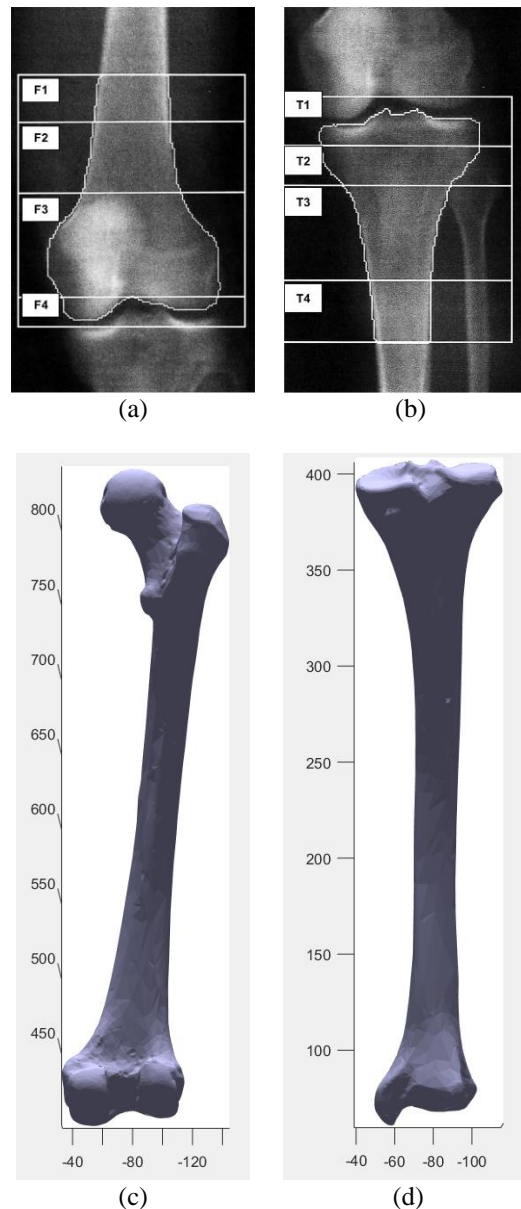

(a)   (b)

(c)   (d)

Figure 4. 3D design of patient-specific implant of total knee joint, (a) analysis of distal femur scan, (b) analysis of proximal tibia scan, (c) femur, (d) tibia

Table 6. Hardness values

Attachment site combination	Range of strainT	Mean of strainT	Standard deviation
F1-T1	24.6–31.9	17.4	9.5
F1-T2	25.4–31.8	17.9	9.5
F1-T3	25.6–40.0	21.7	14
F2-T1	13.9–21.8	13.7	7
F2-T2	27.4–31.0	18.3	9.8
F2-T3	29.7–40	22	11.7

4. CONCLUSION

The tibial implant is designed using a combination of reverse and forward methods, with parametric optimization to minimize stress concentration and ensure optimal force distribution. The optimized 3D-molded tibial implant shows excellent quality, with a smooth surface, no buckling deformation, and minimal adhering slag. While the implant meets strength requirements, its high elasticity modulus has to be addressed through heat treatment in future studies. Further research is needed to refine parametric modeling, structural additive methods, and SLM process parameters, paving the way for directly manufacturing personalized knee implants.

REFERENCES

[1] A. Hedge, "Healthcare 3D Printing Market 2018 Prominent Players-Aprecia Pharmaceuticals, Aspect Biosystems, Bio 3D Technologies, Biobots, Cyfuse Biomedical, Digilab, 3 Dynamics Systems, Envision Tec, Luxexcel, Materialise NV, Nano 3D Biosciences, Oceanz, Organovo Ho," *openPR*, 2018.

[2] C. L. Ventola, "Medical applications for 3D printing: current and projected uses," *Pharmacy and Therapeutics*, vol. 39, no. 10, pp. 704–711, 2014.

[3] D. B. Jones, R. Sung, C. Weinberg, T. Korelitz, and R. Andrews, "Three-dimensional modeling may improve surgical education and clinical practice," *Surgical Innovation*, vol. 23, no. 2, pp. 189–195, 2016, doi: 10.1177/1553350615607641.

[4] M. I. Mohammed, A. P. Fitzpatrick, S. K. Malyala, and I. Gibson, "Customised design and development of patient specific 3D printed whole mandible implant," in *Proceedings of the 27th Annual International Solid Freeform Fabrication Symposium*, Austin, TX, USA, August 2016.

[5] D. C. Ackland, D. Robinson, M. Redhead, P. V. S. Lee, A. Moskaljuk, and G. Dimitoulis, "A personalized 3D-printed prosthetic joint replacement for the human temporomandibular joint: From implant design to implantation," *Journal of the Mechanical Behavior of Biomedical Materials*, vol. 69, pp. 404–411, 2017, doi: 10.1016/j.jmbbm.2017.01.048.

[6] K. Phan, A. Sgro, M. M. Maharaj, P. D'Urso, and R. J. Mobbs, "Application of a 3D custom printed patient specific spinal implant for C1/2 arthrodesis," *Journal of Spine Surgery*, vol. 2, no. 4, pp. 314–318, 2016.

[7] L. E. Diment, M. S. Thompson, and J. H. M. Bergmann, "Clinical efficacy and effectiveness of 3D printing: a systematic review," BMJ Open, vol. 7, no. 12, article e016891, 2017, doi: 10.1136/bmjopen-2017-016891.

[8] J. Garcia, Z. Yang, R. Mongrain, R. L. Leask, and K. Lachapelle, "3D printing materials and their use in medical education: a review of current technology and trends for the future," *BMJ Simulation and Technology Enhanced Learning*, vol. 4, no. 1, pp. 27–40, 2017, doi: 10.1136/bmjstel-2017-000234.

[9] R. J. Mondschein, A. Kanitkar, C. B. Williams, S. S. Verbridge, and T. E. Long, "Polymer structure-property requirements for stereolithographic 3D printing of soft tissue engineering scaffolds," *Biomaterials*, vol. 140, pp. 170–188, 2017, doi: 10.1016/j.biomaterials.2017.06.005.

[10] W. Zhu, X. Ma, M. Gou, D. Mei, K. Zhang, and S. Chen, "3D printing of functional biomaterials for tissue engineering," *Current Opinion in Biotechnology*, vol. 40, pp. 103–112, 2016, doi: 10.1016/j.copbio.2016.03.014.

[11] ASTM, *Standard Technology for Additive Manufacturing- General Principles/Terminology, ASTM ISO/ASTM 52900: 2015 (E)*, West Conshohocken, PA, USA, 2015.

[12] H. J. Chen and M. Gariel, *A roadmap from Idea to Implementation–3D Printing for Pre-Surgical Applications*, CreateSpace Independent Publishing Platform, Scotts Valley, CA, USA, 1st edition, 2012.

[13] A. Cohen, A. Laviv, P. Berman, R. Nashef, and J. Abu-Tair, "Mandibular reconstruction using stereolithographic 3-dimensional printing modeling technology," *Oral Surgery, Oral Medicine, Oral Pathology, Oral Radiology, and Endodontology*, vol. 108, no. 5, pp. 661–666, 2009, doi: 10.1016/j.tripleo.2009.05.023.

[14] D. Whitley, R. S. Eidson, I. Rudek, and S. Bencharit, "In-office fabrication of dental implant surgical guides using desktop stereolithographic printing and implant treatment planning software: a clinical report," *Journal of Prosthetic Dentistry*, vol. 118, no. 3, pp. 256–263, 2017, doi: 10.1016/j.prosdent.2016.10.017.

[15] H. Dodziuk, "Application of 3D printing in healthcare," *Kardiochirurgia i Torakochirurgia Polska*, vol. 13, no. 3, pp. 283–293, 2017, doi: 10.5114/kitp.2016.62625.

[16] D. Ibrahim *et al.*, "Dimensional error of selective laser sintering, three-dimensional printing and PolyJet™ models in the reproduction of mandibular anatomy," *Journal of Cranio-Maxillofacial Surgery*, vol. 37, no. 3, pp. 167–173, 2009, doi: 10.1016/j.jcms.2008.10.008.

[17] "Our 3D Printers". *StrataSys*. Online. [Available]: https://www.sys-uk.com/news/3d-printed-surgical-guides-anddental- implants/.

[18] J. S. Matsumoto *et al.*, "Threedimensional physical modelling: applications and experience at mayo clinic," *RadioGraphics*, vol. 35, no. 7, pp. 1989–2006, 2015, doi: 10.1148/rg.2015140260.

[19] Medtronic case study, Custom surgical instruments becoming working prototypes using FDM 3D printing technology.

[20] K. S. Tanaka and N. Lightdale-Miric, "Advances in 3d-printed pediatric prostheses for upper extremity differences," *Journal of Bone and Joint Surgery*, vol. 98, no. 15, pp. 1320–1326, 2016, doi: 10.2106/jbjs.15.01212.

[21] S. L. Sing, J. An, W. Y. Yeong, and F. E. Wiria, "Laser and electron beam powder-bed additive manufacturing of metallic implants: a review on processes, materials and designs," *Journal of Orthopaedic Research*, vol. 34, no. 3, pp. 369–385, doi: 10.1002/jor.23075.

[22] F. Auricchio and S. Marconi, "3D printing: clinical applications in orthopaedics and traumatology," *EFORT Open Reviews*, vol. 1, no. 5, pp. 121–127, 2016, 10.1302/2058-5241.1.000012.

[23] C. G. Helguero *et al.*, "Biomechanical properties of 3D-printed bone scaffolds are improved by treatment by CRFP," *Journal of Orthopaedic Surgery and Reasearch*, vol. 12, no. 1, p. 195, 2017, doi: 10.1186/s13018-017-0700-2.

[24] M. Asadi-Edyvand, M. Solati-Hasjin, A. Farzad, and N. A. A. Osman, "Effect of technical parameters on porous structure and strength of 3D printed calcium sulfate prototypes," *Robotics and Computer-Integrated Manufacturing*, vol. 37, pp. 57–67, 2015, doi: 10.1016/j.rcim.2015.06.005.

[25] M. S. Mannoor *et al.*, "3D printed bionic ears," *Nano Letters*, vol. 13, no. 6, pp. 2634–2639, 2013, doi: 10.1021/nl4007744.

[26] M. Vukievic, B. Mosadegh, J. K. Min, and S. H. Little, "Cardiac 3D printing and its future directions," *JACC: Cardiovascular Imaging*, vol. 10, no. 2, pp. 171–184, 2017, doi: 10.1016/j.jcmg.2016.12.001.

[27] D. S. C. Soon, M. P. Chae, C. H. C. Pilgrim, W. M. Rozen, R. T. Spychal, and D. J. Hunter-Smith, "3D haptic modelling for

preoperative planning of hepatic resection: a systematic review," *Annals of Medicine and Surgery*, vol. 10, pp. 1–7, 2016, doi: 10.1016/j.amsu.2016.07.002.

[28] I. Abudayyeh, B. Gordon, M. M. Ansari, K. Jutzy, L. Stoletniy, and A. Hilliard, "A practical guide to cardiovascular 3D printing in clinical practice: overview and examples," *Journal of Interventional Cardiology*, vol. 31, no. 3, pp. 375–383, 2017, doi: 10.1111/joic.12446.

[29] M. Cantinotti, I. Valverde, and S. Kutty, "Three-dimensional printed models in congenital heart disease*," International Journal of Cardiovascuolar Imaging*, vol. 33, no. 1, pp. 137–144, 2016, doi: 10.1007/s10554-016-0981-2.

[30] T. Senra, "Dante Pazzanese Cardiology Institute uses 3D printed arteries to diagnose and treat diseases," *Stratasys*, 2020. [Online]. Available: https://www.stratasys.com/en/resources/case-studies/dante-pazzanese/.

[31] R. Burke, "Shaping Young Hearts. Stratasys Helps a Surgeon Save More Kids," *Stratasys*, 2020. [Online]. Available: https://www.stratasys.com/en/resources/case-studies/nicklaus/.

[32] K. Qiu, G. Haghiashtiani, and M. C. McAlpine, "3D printed organ models for surgical applications," *Annual Review of Analytical Chemistry*, vol. 11, no. 1, pp. 287–306, 2018, doi: 10.1146/annurev-anchem-061417-125935.

[33] E. M. Zanetti, A. Aldieri, M. Terzini, M. Calı, G. Franceschini, and C. Bignardi, "Additively manufactured custom loadbearing implantable devices: grounds for caution," *Australasian Medical Journal*, vol. 10, no. 8, pp. 694–700, 2017, doi: 10.21767/amj.2017.3093.

[34] S. N. Kurenov, C. Ionita, D. Sammons, and T. L. Demmy, "Three-dimensional printing to facilitate anatomic study, device development, simulation, and planning in thoracic surgery," *Journal of Thoracic and Cardiovascular Surgery*, vol. 149, no. 4, pp. 973–979, 2015, doi: 10.1016/j.jtcvs.2014.12.059.

[35] H. Jeon *et al.*, "Generation of multilayered 3D structures of HepG2 cells using a bio-printing technique," *Gut and Liver*, vol. 11, no. 1, pp. 121–128, 2017, doi: 10.5009/gnl16010.

[36] M. Randazzo, J. M. Pisapia, N. Singh, and J. P. Thawani, "3D printing in neurosurgery: a systematic review," *Surgical Neurology International*, vol. 7, no. 34, pp. 801–809, 2016, doi: 10.4103/2152-7806.194059.

[37] H. Saijo *et al.*, "Maxillofacial reconstruction using custom-made artificial bones fabricated by inkjet printing technology," *Journal of Artificial Organ*, vol. 12, no. 3, pp. 200–205, 2009, doi: 10.1007/s10047-009-0462-7.

[38] W. Huang and X. Zhang, "3D printing: print the future of ophthalmology," *Investigative Ophthalmology & Visual Science*, vol. 55, no. 8, pp. 5380-5381, 2014, doi: 10.1167/iovs.14-15231.

[39] T. D. Crafts, S. E. Ellsperman, T. J. Wannemuehler, T. D. Bellicchi, T. Z. Shipchandler, and A. V. Mantravadi, "'Three-dimensional printing and its applications in otorhinolaryngology-head and neck surgery," *Otolaryngology-Head and Neck Surgery*, vol. 156, no. 6, pp. 999–1010, 2017, doi: 10.1177/0194599816678372.

[40] M. P. Chae *et al.*, "Emerging applications of bedside 3D printing in plastic surgery," *Frontiers in Surgery*, vol. 16, no. 2, p. 25, 2015, doi: 10.3389/fsurg.2015.00025.

[41] C. Williams, A. James, M. P. Chae, and D. J. Hunter-Smith, "3D printing in clinical podiatry: a pilot study and review," *Journal of Foot and Ankle Research*, vol. 8, no. 2, p. 41, 2015, doi: 10.1186/1757-1146-8-s2-o41.

[42] N. Guilbert *et al.*, "Integration of 3D printing and additive manufacturing in the interventional pulmonologist's toolbox," *Respiratory Medicine*, vol. 134, pp. 139–142, 2018, doi: 10.1016/j.rmed.2017.11.019.

[43] S. Su, K. Moran, and J. L. Robar, "Design and production of 3D printed bolus for electron radiation therapy," *Journal of Applied Clinical Medical Physics*, vol. 15, no. 4, pp. 194–211, 2014, doi: 10.1120/jacmp.v15i4.4831.

[44] N. N. Zein *et al.*, "Three-dimensional print of a liver for preoperative planning in living donor liver transplantation," Liver transplantation, vol. 19, no. 12, pp. 1304–1310, 2013, doi: 10.1002/lt.23729.

[45] Y. Soliman, A. H. Feibus, and N. Baum, "3D printing and its urologic applications," *Urology*, vol. 17, no. 1, pp. 20–24, 2017.

[46] P. Hangge, Y. Pershad, A. A. Witting, H. Albadawi, and R. Oklu, "Three-dimensional (3D) printing and its applications for aortic diseases," *Cardiovascular Diagnosis and Therapy*, vol. 8, no. 1, pp. 19–25, 2018, doi: 10.21037/cdt.2017.10.02.

[47] D. H. Ballard *et al.*, "Clinical applications of 3D printing," *Academic Radiology*, vol. 25, no. 1, pp. 52–65, 2018, doi: 10.1016/j.acra.2017.08.004.

[48] E. Perica and Z. Sun, "Patient-specific three-dimensional printing for pre-surgical planning in hepatocellular carcinoma treatment," *Quantitative Imaging in Medicine and Surgery*, vol. 7, no. 6, pp. 668–677, 2017, doi: 10.21037/qims.2017.11.02.

[49] E. O'Brien, D. B. Wayne, K. A. Barsness, W. C. McGaghie, and J. H. Barsuk, "Use of 3D printing for medical education models in transplantation medicine: a critical review," *Current Transplantation Reports*, vol. 3, no. 1, pp. 109–119, 2016, doi: 10.1007/s40472-016-0088-7.

[50] K. C. Wong, "3D-printed patient-specific applications inorthopedics," *Orthopedic Research and Reviews*, vol. 8, pp. 57–66, 2016, doi: /10.2147/orr.s99614.

[51] J. P. Costello *et al.*, "Incorporating three-dimensional printing into a simulation-based congenital heart-disease and critical care training curriculum for resident physicians," *Congenital Heart Disease*, vol. 10, no. 2, pp. 185–190, 2015, doi: 10.1111/chd.12238.

[52] M. Frame and J. S. Huntley, "Rapid prototyping in orthopaedic surgery: a user's guide," *Scientific World Journal*, vol. 2012, p. 7, 2012, doi: 10.1100/2012/838575.

[53] B. Mahaisavariya, K. Sitthiseripratip, P. Oris, and T. Tongdee, "Rapid prototyping model for surgical planning of corrective osteotomy for cubitus varus: report of two cases," *Injury Extra*, vol. 37, no. 5, pp. 176–180, 2006, doi: 10.1016/j.injury.2005.10.026.

[54] U. Sheth, J. 'eodoropoulos, and J. Abouali, "Use of 3-dimensional printing for preoperative planning in the treatment of recurrent anterior shoulder instability," *Arthroscopy Techniques*, vol. 4, no. 4, pp. 311–316, 2015, doi: 10.1016/j.eats.2015.03.003.

[55] A. Siddiqui, "3D Printing for Vascular Health. Shaping Breakthroughs in Brain Aneurysm Treatments," *Stratasys*.

[56] Y.-T. Wang, X.-J. Yang, B. Yan, T.-H. Zeng, Y.-Y. Qiu, and S.-J. Chen, "Clinical application of three-dimensional printing in the personalized treatment of complex spinal disorders," *Chinese Journal of Traumatology*, vol. 19, no. 1, pp. 31–34, 2016, doi: 10.1016/j.cjtee.2015.09.009.

[57] A. Hosny *et al.* "Pre-procedural fittesting of TAVR valves using parametric modeling and 3D printing," *Journal of Cardiovascular Computed Tomography*, vol. 18, 2018, doi: 10.1016/j.jcct.2018.09.007.

[58] R. Vaishya, V. Vijay, A. Vaish, and A. K. Agarwal, "Computed tomography based 3D printed patient specific blocks for total knee replacement," *Journal of Clinical Orthopaedics and Trauma*, vol. 9, no. 3, pp. 254–259, 2018, doi: 10.1016/j.jcot.2018.07.013.

[59] X. Chen, J. K. Possel, C. Wacongne, A. F. Van Ham, P. C. Klink, and P. R. Roelfsema, "3D printing and modelling of customized implants and surgical guides for non-human primates," *Journal of Neuroscience Methods*, vol. 286, no. 286, pp. 38–55, 2017, doi: 10.1016/j.jneumeth.2017.05.013.

[60] A. De La Pena, J. De La Pena-Brambila, J. Perez-De La Torre, M. Ochoa, and M. J. Gallardo, "Low-cost customized

craniolplasty using a 3D digital printing model: a case report," *3D Printing in Medicine*, vol. 4, no. 1, 2018, doi: 10.1186/s41205-018-0026-7.

[61]   N. Ellerng, "Printing Pathways to Me dical Innovation: 3D Printing's Versatility Paves the Way for Medical Advancements by Cardiovascular Systems, Inc.," Stratasys, Jul. 2018. [Online]. Available: https://www.stratasys.com/en/resources/case-studies/cardiovascular-systems/.

BIOGRAPHIES OF AUTHORS

Bolugoddu Sandeep is a research scholar in the Department of Mechanical Engineering at PRIST Deemed to be University, Tamil Nadu, India. His research area focuses on additive manufacturing, under the guidance of Dr. S. Dhanushkodi. Enrolled in 2019, he has contributed to the field through his publication titled "Scope of 3D Printing in Manufacturing Industries - A Review." This work explores the potential applications and advancements of 3D printing technologies in the manufacturing sector, highlighting their transformative impact on industrial processes. He can be contacted at email: sandeepvarma@jits.in.

Dr. Saravanan Dhanushkodi is the Dean of Engineering and Technology at PRIST University in Thanjavur. He has published 16 publications and has been cited by 320 people. He has published several research papers in various International Journals and International/Nationalconferences, has also attended several national and international conferences and workshops. He can be contacted at email: dhanushkodi.vs@gmail.com.

Dr. Sudhakar Kumarasamy is currently an Associate Professor at the Faculty of Mechanical and Automotive Engineering Technology, Universiti Malaysia Pahang, and Principal Research Fellow at the Centre for Automotive Engineering. He has held several visiting faculty and researcher positions at universities in India, Russia, Lithuania, Nepal, and Vietnam.He earned his Bachelor in Mechanical Engineering from the Government College of Engineering, Salem, University of Madras in 2001, and his Masters in Energy Management from the School of Energy and Environment Studies, Devi Ahilya University, Indore in 2006. He received his Ph.D. in Energy Engineering from the National Institute of Technology, Tiruchirapalli, India in 2013. He can be contacted at email: sudhkar@umpsa.edu.my.